

# Cross-Layer Vision Smoothing: Enhancing Visual Understanding via Sustained Focus on Key Objects in Large Vision-Language Models

Jianfei Zhao<sup>1,2</sup>, Feng Zhang<sup>1</sup>, Xin Sun<sup>1</sup>, Lingxing Kong<sup>4</sup>, Zhixing Tan<sup>4</sup>, Chong Feng<sup>1,3</sup>

<sup>1</sup>School of Computer Science and Technology, Beijing Institute of Technology

<sup>2</sup>Zhongguancun Academy

<sup>3</sup>Southeast Academy of Information Technology, Beijing Institute of Technology

<sup>4</sup>Tsinghua University

{zhqingan, bit\_zhangfeng, sunxin}@bit.edu.cn, klxstar@126.com, tzx.2019@tsinghua.org.cn, fengchong@bit.edu.cn

## Abstract

Large Vision-Language Models (LVLMs) can accurately locate key objects in images, yet their attention to these objects tends to be very brief. Motivated by the hypothesis that sustained focus on key objects can improve LVLMs' visual capabilities, we propose Cross-Layer Vision Smoothing (CLVS). The core idea of CLVS is to incorporate a vision memory that smooths the attention distribution across layers. Specifically, we initialize this vision memory with position-unbiased visual attention in the first layer. In subsequent layers, the model's visual attention jointly considers the vision memory from previous layers, while the memory is updated iteratively, thereby maintaining smooth attention on key objects. Given that visual understanding primarily occurs in the early and middle layers of the model, we use uncertainty as an indicator of completed visual understanding and terminate the smoothing process accordingly. Experiments on four benchmarks across three LVLMs confirm the effectiveness and generalizability of our method. CLVS achieves state-of-the-art performance on a variety of visual understanding tasks, with particularly significant improvements in relation and attribute understanding.<sup>1</sup>

## 1 Introduction

Large Vision-Language Models (LVLMs) (Liu et al. 2023; Bai et al. 2025) acquire the capability to comprehend visual information through training on large-scale multimodal data and exhibit strong performance across a wide range of visual understanding tasks (Li et al. 2023; Wang et al. 2023; Fu et al. 2024). Despite these successes, LVLMs still suffer from issues such as hallucinations (Leng et al. 2024), which limit their real-world applications.

Recent studies (Zhang et al. 2025; Chen et al. 2025) have revealed a strong correlation between the visual understanding capability of LVLMs and their visual attention. Visual attention is learned through end-to-end training without direct supervision. While this approach simplifies LVLM training, it also makes it difficult to avoid biases in visual attention (Liu, Zheng, and Chen 2024; Kang et al. 2025; Zhu et al. 2025b), such as position bias (Zhu et al. 2025b; Li et al. 2025), visual attention sink (Huang et al. 2024; Kang et al. 2025), and uncoordinated attention heads (He et al. 2025; Yang et al. 2025). Consequently, a series of recent works

have sought to enhance the visual understanding capabilities of LVLMs by improving visual attention. Liu, Zheng, and Chen (2024); Zhu et al. (2025a); Yin, Si, and Wang (2025a) propose directly increasing the attention weights on visual tokens. Yang et al. (2025); He et al. (2025) analyze the effect of the multi-head attention mechanism on visual understanding and remove attention heads that negatively impact performance. Kang et al. (2025); Xie et al. (2025); Chen et al. (2025) adjust the visual attention distribution to achieve finer control over the model's visual understanding process. These successes confirm the crucial role of visual attention in the visual understanding of LVLMs.

While previous studies have demonstrated effectiveness in improving the visual attention of LVLMs, they primarily focus on enhancing attention within individual layers without considering the cross-layer evolution of visual attention. We observe that visual attention can change dramatically between consecutive layers. For example, in Figure 1, when asked “Is the woman wearing a black shirt?”, the model attends to the “woman” and “shirt” (*i.e.*, key objects) at layer 14 but ceases to focus on them afterward. Although the model accurately locates key objects, its attention to these objects is very brief. This phenomenon, commonly observed across different LVLMs and images, is referred to as *advantageous attention decay*. We hypothesize that such brief attention is insufficient for effective visual information fusion in LVLMs. Therefore, sustaining an appropriate focus on key objects is beneficial to enhance the model's visual capabilities.

To tackle advantageous attention decay, we propose Cross-Layer Vision Smoothing (CLVS) to enhance LVLMs' visual comprehension by maintaining sustained focus on key objects in the image. To this end, we introduce a vision memory for smoothing visual attention across layers. Specifically, following Li et al. (2025), we unify the visual attention in the first layer for unbiased perception and initialize the vision memory with the visual attention distribution. In subsequent layers, we progressively smooth visual attention by interpolating it with the vision memory and updating the memory iteratively. Moreover, since visual understanding primarily occurs in the early and middle layers of LVLMs, we propose an uncertainty-based criterion to determine whether the visual understanding process has been completed and, if so, terminate visual attention smoothing.

<sup>1</sup>Our code is available at <https://github.com/beta-nlp/CLVS>.

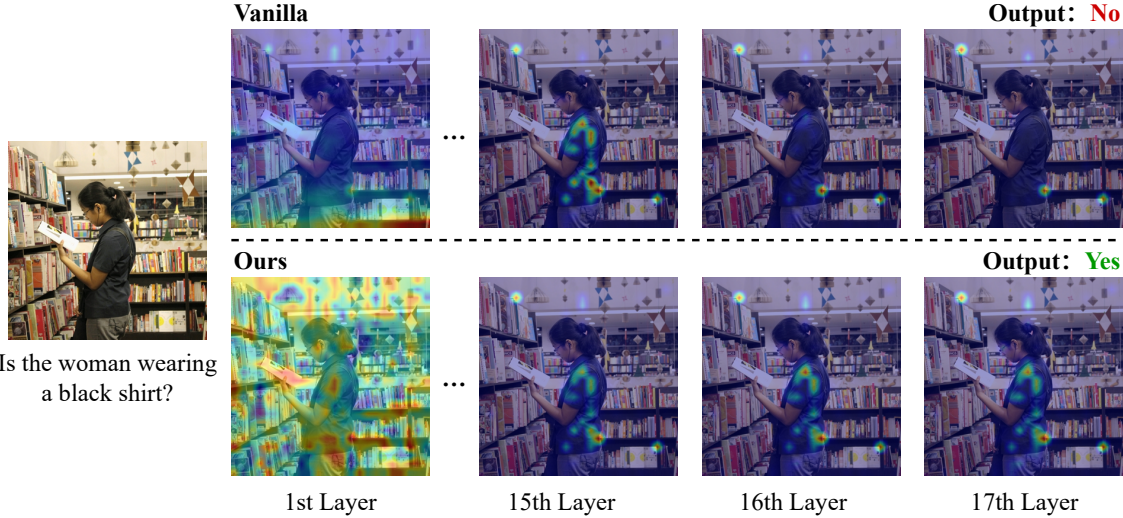


Figure 1: A running example of visual attention in LLaVA-1.5-7B. In vanilla LVLMs, first-layer attention is biased toward the bottom, and focus on the key object (woman) decays after layer 15.

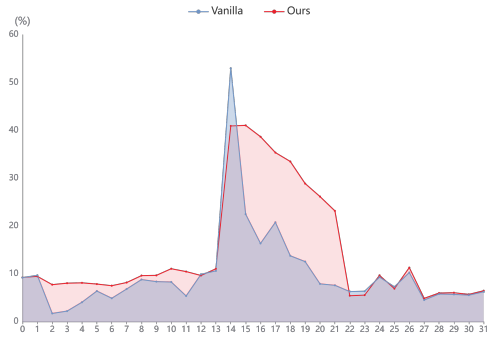


Figure 2: Comparison of visual attention to key objects across layers between LVLMs with and without CLVS.

With CLVS, the model can sustain focus on key objects, thereby improving the visual capabilities of LVLMs. The comparison of visual attention to key objects across layers between LVLMs with and without CLVS is shown in Figure 2.

We conduct extensive experiments on four visual understanding benchmarks and three LVLMs. The results demonstrate that CLVS effectively improves the visual capabilities of LVLMs, reducing hallucinations, particularly those related to object attributes and relations.

In summary, our contributions are:

- We analyze the cross-layer evolution of visual attention and identify advantageous attention decay, a phenomenon where the model's focus on key objects is short-lived.
- We propose Cross-Layer Vision Smoothing (CLVS), which sustains the model's focus on key objects to enhance visual understanding.

- We conduct extensive experiments and in-depth analyses to show that CLVS effectively alleviates advantageous attention decay and reduces hallucinations, particularly those related to object attributes and relations.

## 2 Related Work

The cross-modal understanding ability of LVLMs is built upon the attention mechanism. However, end-to-end training lacks supervision over the model's internal processes, leading to shortcomings in the spontaneously formed visual attention, such as position bias and visual attention sink. These issues can result in hallucinations (Liu et al. 2024; Zhao et al. 2025b) in the model's output.

Numerous works have explored improving visual attention in LVLMs. Yang et al. (2025); Zhu et al. (2025b) incorporate supervisory signals into the attention mechanism, enabling fine-grained control during training. To avoid high training costs and improve generalizability, an increasing number of studies focus on training-free approaches to optimize visual attention. Given the critical role of visual information in LVLMs, Liu, Zheng, and Chen (2024); Zhu et al. (2025a); Yin, Si, and Wang (2025a) directly increase the model's attention weights on visual tokens. While effective, these approaches overlook the internal dynamics of visual attention. Leveraging the diversity of multi-head attention, Zhang et al. (2024); Zhao et al. (2025a); Yang et al. (2025) identify and utilize high-quality attention heads to optimize visual attention. Recent studies (Kang et al. 2025; Xie et al. 2025) further analyze attention distributions to identify the causes of hallucinations and implement targeted optimizations. However, these works enhance visual attention independently within each layer, overlooking its evolution across layers.

Different from the above approaches, we propose CLVS

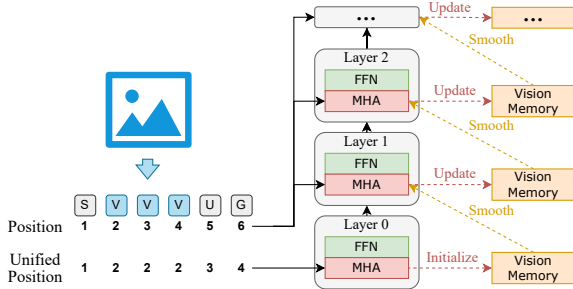


Figure 3: Overview of CLVS.  $S$ ,  $V$ ,  $U$ , and  $G$  denote system tokens, visual tokens, user tokens, and the current generating token, respectively. Unified position indices are applied in the first layer. The vision memory, initialized from this unbiased visual attention, smooths and is updated across subsequent layers.

to maintain a sustained focus on key objects throughout the model. Our method introduces a vision memory to smooth attention distributions across layers, ensuring continuous focus on key objects and enhancing the visual capabilities of LVLMs.

### 3 Cross-Layer Vision Smoothing

To ensure sustained attention to key objects in the image, we propose Cross-Layer Vision Smoothing (CLVS). Figure 3 provides an overview of our method. We first normalize the positional relationships between visual tokens in the initial layer, then initialize a vision memory with unbiased visual attention. This vision memory smooths the visual attention and is dynamically updated across subsequent layers. Finally, the smoothing mechanism is terminated once the model completes the visual understanding process.

#### 3.1 Unified Visual Positions

Given a Transformer-based LVLM  $f_\theta$  with parameters  $\theta$ , the goal of the model is to predict the next-token distribution given textual inputs  $\mathbf{x}$ , visual inputs  $\mathbf{v}$ , and previously generated texts  $\mathbf{y} < t$ , which can be formulated as

$$p(y_t | \mathbf{x}, \mathbf{v}, \mathbf{y}_{<t}) = f_\theta(\mathbf{x}, \mathbf{v}, \mathbf{y}_{<t}). \quad (1)$$

The LVLM employs an embedding layer and a vision encoder to map both text and images into a sequence of vectors. Positional embeddings are then added to establish contextual relationships among the tokens.

Positional embeddings are determined by the absolute or relative position of a token in a sequence and play an important role in Transformer-based models. Recent studies (Zhu et al. 2025b; Li et al. 2025) have found that Transformer-based LVLMs tend to focus disproportionately on the bottom-right corner of the image (*i.e.*, the visual tokens at the end of the input sequence), a bias influenced by the positions of visual tokens in the inputs. Unlike textual inputs, visual information does not inherently possess sequential characteristics. Therefore, the model should receive

unbiased attention, particularly in the first layer, where it has no prior visual perception.

Following Li et al. (2025), we normalize the positional indices of all image tokens to a unified index and replace the original positional indices in the concatenated input sequence. Given a sequence of length  $N = N_s + N_v + N_i$ , the new positional indices are formally defined as

$$\mathbf{p} = [\{i\}_{i=0}^{N_s}, \{N_s + 1\}_{i=0}^{N_v}, \{i + 1\}_{i=N_s+1}^{(N_s+N_v)}], \quad (2)$$

where  $N_s$ ,  $N_v$ , and  $N_i$  denote the number of tokens in the system prompt, image, and user prompt, respectively. Note that since we only adjust the visual attention of the current generating token, the unified position does not affect the attention among visual tokens. Because of the causal mask in the attention layer, information flows unidirectionally through the input sequence (Zhao et al. 2025a; Yin, Si, and Wang 2025b), which aligns with the positional indices. Therefore, we apply position debiasing to the input image only in the first layer.

#### 3.2 Visual Attention Smoothing

The multi-head attention layers aggregate information from the sequence of vectors into a single representation through a weighted sum. Formally, at decoding step  $t$ , given a query vector  $\mathbf{q} \in \mathbb{R}^d$  where  $d$  is the hidden size of  $f$ , and a set of key vectors  $\mathbf{K} \in \mathbb{R}^{N \times d}$  where  $N$  is the sequence length of all tokens, the attention weights  $\alpha_h^{(l)} \in \mathbb{R}^N$  computed by head  $h$  at layer  $l$  are defined as

$$\alpha_h^{(l)} = \text{softmax}\left(\frac{\mathbf{q}\mathbf{K}^\top}{\sqrt{d}}\right). \quad (3)$$

Previous studies (Zhang et al. 2025; Chen et al. 2025) reveal a strong correlation between the visual understanding capabilities of LVLMs and their visual attention. However, we found that the model’s attention quickly converges on sink tokens, hindering sustained focus on key objects. To mitigate this issue and ensure stable attention on key objects, we introduce a vision memory  $\mathbf{m}$  into the LVLM, which serves as a cross-layer smoothing mechanism in visual attention. Let  $\alpha_h^{(l)} = \{\lambda_h^{(l)}, \mu_h^{(l)}\}$ , where  $\lambda_h^{(l)} \in \mathbb{R}^{N_v}$  denotes the attention weights associated with visual tokens ( $N_v$  is the number of visual tokens), and  $\mu_h^{(l)} \in \mathbb{R}^{N - N_v}$  denotes the attention weights associated with non-visual tokens. The vision memory  $\mathbf{m}$  stores only the attention weights corresponding to visual tokens. We initialize the vision memory at the first layer, denoted as  $\mathbf{m}^{(1)}$ , using the unbiased visual attention of that layer, and apply max pooling across attention heads to compress the model’s overall attention to the image:

$$\mathbf{m}^{(1)}[i] = \max_{1 \leq h \leq H} \lambda_h^{(1)}[i], \quad (4)$$

where  $\mathbf{m}^{(1)}[i] \in \mathbb{R}$  denotes the  $i$ -th element of  $\mathbf{m}^{(1)}$ ,  $H$  is the total number of attention heads, and  $i \in \{1, \dots, N_v\}$ . This highlights the most salient visual information captured at each layer and propagates it across different attention heads.

In the subsequent Transformer layers, we smooth the visual attention weights for each head and update the vision memory iteratively. The smoothing formula for visual attention is formally defined as

$$\hat{\lambda}_h^{(l)} = \beta \lambda_h^{(l)} + (1 - \beta) \mathbf{m}^{(l-1)}, \quad 1 \leq h \leq H, \quad (5)$$

where  $\beta \in [0, 1]$  is a hyperparameter that controls the extent of smoothing. However, smoothing the visual attention weights may invalidate the normalization property of  $\alpha_h^{(l)}$ , so we need to re-normalize the attention scores. Since directly re-normalizing the attention distribution with the softmax function may reduce its sharpness, we instead apply a simple re-normalization by:

$$\hat{\alpha}_h^{(l)}[i] = \frac{\alpha_h^{(l)}[i]}{\sum_{k=1}^n \alpha_h^{(l)}[k]}, \quad 1 \leq h \leq H. \quad (6)$$

The vision memory is then updated layer by layer based on the original visual attention from each layer:

$$\mathbf{m}^{(l)}[i] = \gamma \mathbf{m}^{(l-1)}[i] + (1 - \gamma) \max_{1 \leq h \leq H} \lambda_h^{(l)}[i], \quad (7)$$

where  $\gamma \in [0, 1]$  is the soft memory window size that limits how far the model can look back into previous vision memories. A larger  $\gamma$  allows the model to access more distant vision memories across layers.

Since the vision memory is initialized with unbiased visual attention, our method allows the model to capture more visual information in the early layers. Once the model identifies key objects, the smoothing mechanism slows the decay of visual attention, enabling sustained focus on those objects.

### 3.3 Vision Understanding Completion

The visual understanding process in LVLMs primarily occurs in the early and middle layers, while language-level feature construction takes place in the final layers (Yin, Si, and Wang 2025b; Zhao et al. 2025a). Therefore, adjustments to visual attention should target the early and middle layers. Previous works (Xie et al. 2025; Yin, Si, and Wang 2025a) often determine the layer range for attention optimization by setting fixed hyperparameters, which limits generalization across different LVLMs. To address this, we propose a dynamic mechanism that determines the active layer range by assessing whether the model’s visual understanding process is complete, and terminates CLVS accordingly.

Intuitively, if the model’s output has converged (*i.e.*, the output token remains unchanged in subsequent layers under greedy decoding), we can terminate the smoothing process. However, output convergence is determined based on the final layer’s output and therefore cannot be known at the current layer. A straightforward approach would be to perform a preliminary forward pass to determine the convergence status at each layer, but this significantly increases inference cost. Following Zou et al. (2025), we instead use output uncertainty at each layer as a surrogate measure to determine the end of visual understanding. Specifically, we multiply the representation by the unembedding matrix to obtain the

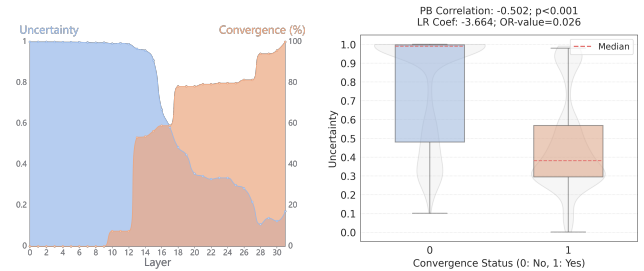


Figure 4: Statistical results of output uncertainty and convergence on the MME benchmark. Left: clear inverse relationship between convergence and uncertainty. Right: “PB Correlation” denotes Point-Biserial Correlation, and “LR Coefficient” denotes the coefficient from Logistic Regression analysis.

probability distribution at the current layer  $l$ , and calculate the uncertainty measure  $u$  as

$$u = \frac{\sum_{k=1}^{|V|} -p_t \log p_t}{\log |V|}, \quad (8)$$

where  $|V|$  denotes the vocabulary size. For computational concerns, we follow the practice of Zou et al. (2025) and compute only the top-10 tokens (*i.e.*,  $|V| = 10$ ).

We analyze the uncertainty and convergence of the model’s responses, with results shown in Figure 4. From the left panel, we observe a strong correlation between convergence and uncertainty: as uncertainty decreases, the model progressively completes visual perception and begins constructing semantic information. Both point-biserial correlation and logistic regression analyses, shown in the right panel, further confirm statistical associations between these measures. Based on these observations, we use uncertainty to determine whether the model has completed visual perception. Since this process is completed by at least the middle layers, we introduce uncertainty detection starting from the  $(L + 1)/2$ -th layer to avoid unnecessary computations. Visual attention smoothing is terminated in subsequent Transformer layers once the uncertainty falls below the threshold  $\delta$ .

## 4 Experiments

### 4.1 Setup

**Benchmarks.** We use the following benchmarks to test the effectiveness of our method:

- **AMBER** (Wang et al. 2023): a human-annotated benchmark including three types of hallucination evaluation questions: existence, attribute, and relation.
- **R-Bench** (Wu et al. 2024): a benchmark for evaluating relation hallucination, which pose a greater challenge to the model’s visual understanding ability. This benchmark provides multiple randomly constructed subsets with a balanced number of *Yes* and *No* questions, and we use the subset with ID 1. We conduct experiments using image-level questions.

Model	Method	Existence		Attribute		Relation		All	
		Acc.	F1	Acc.	F1	Acc.	F1	Acc.	F1
LLaVA-1.5-7B	Vanilla	71.4	83.3	72.0	64.4	74.1	68.5	72.1	74.8
	VCD (Leng et al. 2024)	68.3	81.1	<b>72.7</b>	<b>66.6</b>	72.4	65.1	71.1	74.1
	PAI (Liu, Zheng, and Chen 2024)	<u>75.7</u>	<u>86.1</u>	71.9	64.2	<u>75.8</u>	<u>71.2</u>	<u>73.7</u>	<u>76.7</u>
	VAR (Kang et al. 2025)	70.7	82.8	72.1	65.0	73.7	66.6	71.8	74.6
	AD-HH (Yang et al. 2025)	71.4	83.3	71.8	64.2	74.0	68.7	71.9	74.8
	VAF (Yin, Si, and Wang 2025a)	64.4	78.3	70.4	61.7	73.3	65.3	68.7	70.9
	TARAC (Xie et al. 2025)	72.1	83.7	71.4	63.5	74.2	68.4	72.0	74.8
	CLVS	<b>77.6</b>	<b>87.3</b>	<b>72.7</b>	<b>65.4</b>	<b>77.1</b>	<b>73.7</b>	<b>75.0</b>	<b>78.1</b>
LLaVA-1.5-13B	Vanilla	66.0	79.5	75.3	69.5	70.1	45.2	71.5	73.5
	VCD (Leng et al. 2024)	64.6	78.4	75.9	71.3	69.9	45.7	71.3	73.5
	PAI (Liu, Zheng, and Chen 2024)	<u>70.5</u>	<u>82.6</u>	<u>78.1</u>	<u>74.3</u>	<u>73.9</u>	<u>56.6</u>	<u>75.0</u>	<u>77.6</u>
	VAR (Kang et al. 2025)	65.2	78.9	75.1	69.1	69.7	43.8	71.0	72.9
	AD-HH (Yang et al. 2025)	67.1	80.3	75.8	70.4	70.0	45.5	72.1	74.2
	VAF (Yin, Si, and Wang 2025a)	61.4	76.0	74.9	68.9	69.4	43.5	69.5	71.2
	TARAC (Xie et al. 2025)	68.7	81.4	76.2	70.9	71.3	48.7	73.0	75.3
	CLVS	<b>78.4</b>	<b>87.8</b>	<b>78.9</b>	<b>76.7</b>	<b>76.2</b>	<b>64.3</b>	<b>78.4</b>	<b>81.8</b>
LLaVA-Next	Vanilla	<b>95.1</b>	<b>97.4</b>	84.0	85.0	67.2	71.5	85.9	89.8
	VCD (Leng et al. 2024)	95.0	<b>97.4</b>	84.4	85.2	67.7	71.8	86.1	89.9
	VAF (Yin, Si, and Wang 2025a)	93.0	96.3	84.7	85.3	71.5	74.2	86.0	89.7
	TARAC (Xie et al. 2025)	95.0	<b>97.4</b>	84.2	85.1	66.2	70.9	85.8	89.8
	CLVS	93.5	96.6	<b>85.2</b>	<b>85.7</b>	<b>72.1</b>	<b>74.5</b>	<b>86.6</b>	<b>90.0</b>
Qwen2.5-VL	Vanilla	95.3	97.5	83.5	84.4	73.9	75.8	86.5	90.1
	VCD (Leng et al. 2024)	93.0	96.3	83.7	84.3	73.3	75.0	85.7	89.4
	VAF (Yin, Si, and Wang 2025a)	93.8	96.8	83.7	84.5	71.5	74.1	85.7	89.5
	TARAC (Xie et al. 2025)	<b>95.4</b>	<b>97.6</b>	83.5	84.5	73.6	75.6	86.5	90.1
	CLVS	94.8	97.3	<b>83.9</b>	<b>84.8</b>	<b>74.6</b>	<b>76.2</b>	<b>86.6</b>	<b>90.2</b>

Table 1: Results on AMBER. **Bold** indicates the best result in each setting, and underline indicates the second best. “All” denotes the aggregated results over all test samples.

We also conduct experiments on the following benchmarks to further validate our proposed CLVS method:

- **POPE** (Li et al. 2023): a benchmark for evaluating existence hallucination. It consists of three subsets: *Random*, *Popular*, and *Adversarial*, each constructing negative examples in a distinct manner.
- **MME** (Fu et al. 2024): a comprehensive evaluation benchmark. We use perception tasks to test the model’s visual understanding ability following previous works, which includes four types of questions: *Existence*, *Color*, *Count*, and *Position*.

**Baselines.** We compare our method with the following baselines:

- **VCD** (Leng et al. 2024): a method that stimulates visual uncertainty by adding noise to images and purifies visual information using contrastive decoding.
- **PAI** (Liu, Zheng, and Chen 2024): a method that directly amplifies visual attention and performs contrastive decoding with pure textual context to purify visual information.
- **VAR** (Kang et al. 2025): a method that identifies visual sink tokens and redistributes the model’s attention from sink tokens to other visual tokens.

- **AD-HH** (Yang et al. 2025): a method that identifies attention heads that cause hallucinations. When the attention of these heads to text exceeds a threshold, their attention to text is set to zero, thereby enhancing visual attention.
- **VAF** (Yin, Si, and Wang 2025a): a method that redistributes the model’s attention from system tokens to visual tokens in the middle layers where the model performs visual understanding.
- **TARAC** (Xie et al. 2025): a method that also optimizes visual attention in the middle layers. It accumulates visual attention from each generation step and injects it into the visual attention of the current step.

The implementation details of baselines are provided in the Appendix A.

**Implementation Details.** In all experiments, LVLMs use greedy search for next-token prediction. We set  $\beta = 0.8$  in Eq. (5) for all LVLMs. The value of  $\gamma$  in Eq. (7) is set to 0.8 for LLaVA-1.5, 0.7 for LLaVA-Next and Qwen2.5-VL. The setting of uncertainty threshold  $\delta$  is based on the statistical analysis (see Figure 4), with a value of 0.5. All models are tested at the 7B or 8B parameter scale unless explicitly stated otherwise. We conduct our experiments on a single NVIDIA A800 40G GPU.

Method	Acc.	Prec.	Rec.	F1	Acc.	Prec.	Rec.	F1
	LLaVA-1.5-7B				LLaVA-1.5-13B			
Vanilla	67.8	61.6	95.3	74.8	68.2	61.7	<u>96.9</u>	75.4
VCD (Leng et al. 2024)	68.2	62.1	94.6	75.0	68.9	62.5	95.2	75.5
PAI (Liu, Zheng, and Chen 2024)	<u>68.7</u>	<u>62.4</u>	95.3	<u>75.4</u>	<u>71.0</u>	<u>64.2</u>	95.9	<u>76.9</u>
VAR (Kang et al. 2025)	68.0	61.8	95.2	75.0	68.0	61.5	<b>97.0</b>	75.3
AD-HH (Yang et al. 2025)	67.6	61.5	95.4	74.8	68.6	62.1	96.7	75.6
VAF (Yin, Si, and Wang 2025a)	66.8	60.7	<b>96.2</b>	74.5	67.7	61.3	<u>96.9</u>	75.1
TARAC (Xie et al. 2025)	67.7	61.5	95.5	74.8	68.8	62.2	96.7	75.7
CLVS	<b>69.0</b>	<b>62.5</b>	<u>95.7</u>	<b>75.6</b>	<b>71.3</b>	<b>64.6</b>	95.2	<b>77.0</b>
	LLaVA-Next				Qwen2.5-VL			
Vanilla	<b>81.9</b>	80.1	85.3	82.6	81.6	80.2	<b>84.2</b>	82.1
VCD (Leng et al. 2024)	80.2	78.3	83.8	81.0	79.5	78.3	82.1	80.1
VAF (Yin, Si, and Wang 2025a)	81.3	78.2	<b>87.0</b>	82.4	81.5	80.7	83.1	81.9
TARAC (Xie et al. 2025)	81.8	<b>80.3</b>	84.5	82.3	81.6	<b>80.9</b>	83.1	82.0
CLVS	<b>81.9</b>	79.3	86.6	<b>82.8</b>	<b>81.8</b>	80.4	<b>84.2</b>	<b>82.3</b>

Table 2: Results on R-Bench. ‘‘Prec.’’ and ‘‘Rec.’’ denote Precision and Recall, respectively.

Method	Accuracy	Recall	F1
LLaVA-Next			
Vanilla	87.39	77.09	85.94
CLVS	<b>88.49</b> (+1.10)	<b>79.78</b> (+2.69)	<b>87.39</b> (+1.45)
Qwen2.5-VL			
Vanilla	89.91	82.87	89.15
CLVS	<b>90.16</b> (+0.25)	<b>83.07</b> (+0.20)	<b>89.40</b> (+0.25)

Table 3: Results on the *Random* subset in POPE.

## 4.2 Main Results

**Results on AMBER.** Table 1 shows the results on AMBER, a comprehensive hallucination evaluation benchmark that includes tests for three major types of hallucinations. Our method achieves notable improvements over baselines on multiple LVLMs, particularly in understanding object relationships. Compared with other tasks, the improvement in determining object existence is relatively small, especially when using models such as Qwen2.5-VL and LLaVA-Next, which possess stronger visual comprehension capabilities. This is because our approach leverages the inherent attention advantages of LVLMs to maintain focus on key objects, thereby substantially enhancing performance in complex relational reasoning. However, in object-existence determination tasks where relevant objects may be absent from the image, our method cannot establish focused attention on key objects and thus provides limited improvements.

**Results on R-Bench.** Table 2 shows the results on the R-Bench benchmark. Our method achieves significant improvements in evaluating relational hallucinations, attaining state-of-the-art F1 scores across all LVLMs, including strong models such as Qwen2.5-VL and LLaVA-Next. These results are consistent with those on AMBER, further demonstrating the versatility of our method.

VCD PAI VAR AD-HH VAF TARAC CLVS (Ours) Total

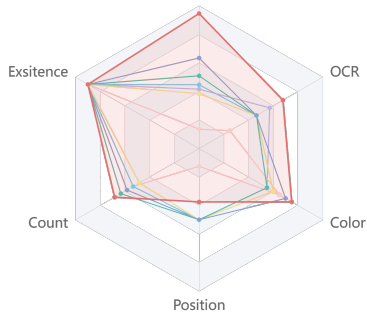


Figure 5: Radar chart of results on the MME benchmark.

## 4.3 Results on POPE

As discussed earlier, our method provides limited improvements when key objects are absent from the image. For example, when the answer to the question ‘‘*Is there a/an {object} in the image?*’’ is ‘‘*False*’’, there are no relevant key objects to attend to, which limits the effectiveness of our approach. To further examine this issue, we conduct additional experiments on the POPE dataset, a benchmark designed for existence hallucination. The results are presented in Table 3. We find that while our method does not yield substantial gains in accuracy, it achieves a notable increase in recall. This indicates that when key objects are present, our method effectively enhances the model’s visual understanding by sustaining attention on them.

## 4.4 Results on MME

We further evaluate our method on a broader range of tasks using the MME benchmark, with results shown in Figure 5. Our method achieves the highest overall score among all baselines except on the position task. We conjecture that the position task relies heavily on spatial information in the image, while our approach primarily prolongs LVLMs’ focus

Method	Acc.	Prec.	Rec.	F1
CLVS	<b>75.0</b>	<b>93.3</b>	<b>67.1</b>	<b>78.1</b>
w/o Early Termination	74.9	<b>93.3</b>	67.0	78.0
w/o Unified Position	74.8	93.1	67.0	77.9

Table 4: Ablation Study on AMBER with LLaVA-1.5-7B. “w/o Early Termination” represents performing vision smoothing until the final layer. “w/o Unified Position” represents employ original position indices in the first layer.

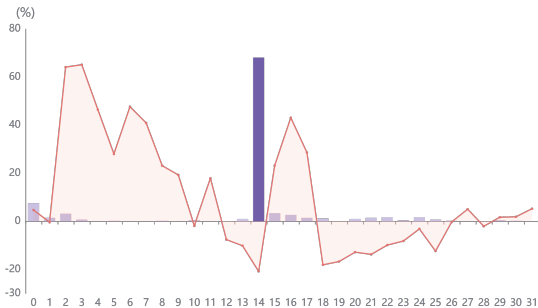


Figure 6: Statistical results of visual attention on key objects in LLaVA-1.5. The bar chart shows the distribution of attention peaks across layers in the vanilla method, while the line chart shows the average increase in attention on key objects by CLVS relative to vanilla in each layer.

on key objects and therefore does not enhance their understanding of spatial relationships. Nevertheless, our method yields significant improvements on the color and count tasks, where key objects are present.

#### 4.5 Ablation Study

We conduct an ablation study on CLVS, with results presented in Table 4. We observe positive contributions from both unified positional indices and early termination. For unified positional indices, the improvements are considerably smaller than those achieved by vision smoothing, since this operation is applied only in the first layer and its influence gradually diminishes during subsequent smoothing. Therefore, simply increasing the amount of information attended to by altering positional indices does not directly enhance visual understanding. Regarding early smoothing termination, we confirm that it has no negative impact on model performance, consistent with previous findings that visual understanding in LLMs primarily occurs in the early and middle layers. Thus, early termination reduces computational cost without sacrificing performance. As a result, we confirm the effectiveness of all elements in our CLVS.

#### 4.6 Analysis

**Key Object Attention Analysis.** To validate the effectiveness of CLVS in strengthening advantageous visual attention, we conduct experiments on 500 positive samples from POPE and use manually annotated instance segmentations from the MSCOCO dataset to localize key objects.

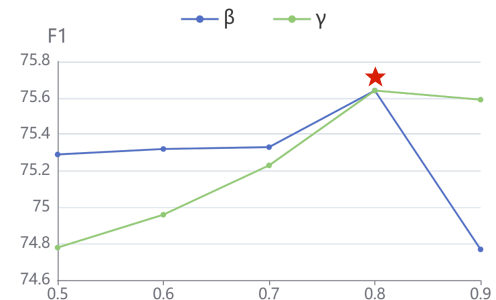


Figure 7: Performance of CLVS with varying values of  $\beta$  and  $\gamma$ . We vary  $\beta$  while fixing  $\gamma$  at 0.8, and similarly vary  $\gamma$  while fixing  $\beta$  at 0.8.

We measure the attention to a key object in layer  $l$  using  $a_{\text{obj}}^{(l)} = \sum_{i=1}^{N_v} \mathbf{a}^{(l)}[i] \cdot \frac{\text{Area}(\text{patch}_i \cap \text{obj})}{\text{Area}(\text{patch}_i)}$ , where  $N_v$  is the number of visual tokens and  $\mathbf{a}^{(l)}[i]$  is the average attention value for visual token  $i$  across attention heads. We analyze the peak-layer distribution  $l_p$  ( $l_p = \text{argmax}_l a_{\text{obj}}^{(l)}$ ) and the relative increase of  $a_{\text{obj}}^{(l)}$  in CLVS over vanilla method (clipped at 100%). The statistical results are shown in Figure 6. In the vanilla method, attention to key objects typically emerges around layer 14 but quickly diminishes, consistent with prior findings (Zhang et al. 2025). In contrast, CLVS sustains focus on key objects, as evidenced by a large relative increase in attention weights in the lower layers, with an average gain of 31.65% from layers 15 to 17. Since early smoothing termination is applied starting in the middle layers, the model no longer preferentially attends to key objects above these layers. This enhanced attention facilitates better understanding of object-related information, enabling CLVS to reduce attribute and relation hallucinations.

**Effects of  $\beta$  and  $\gamma$ .**  $\beta$  and  $\gamma$  are two important hyperparameters that directly affect the performance of our method. We conduct experiments by varying their values, with results shown in Figure 7. We find a notable drop in performance when  $\beta$  approaches 1 (with  $\gamma$  fixed at 0.8), as the vision memory plays a smaller role in smoothing the visual attention distribution. We also observe a performance drop when  $\gamma$  is small (with  $\beta$  fixed at 0.8), since the vision memory may update too frequently. Very large or very small values of  $\beta$  cause dramatic changes in the attention distributions across layers. These results are consistent with our hypothesis that sustained focus on key objects is essential.

## 5 Conclusion

In this paper, we propose Cross-Layer Vision Smoothing (CLVS) to mitigate advantageous attention decay in LLMs. CLVS initializes a vision memory with unified visual positional indices in the first layer, which is then refined and updated across subsequent layers. Using output uncertainty, we adaptively terminate smoothing once visual perception is complete, thereby reducing redundant computation. Ex-

periments demonstrate that CLVS sustains attention on key objects and enhances visual understanding.

## Acknowledgments

This work is supported by Zhongguancun Academy Project No.20240103.

## References

Bai, S.; Chen, K.; Liu, X.; Wang, J.; Ge, W.; Song, S.; Dang, K.; Wang, P.; Wang, S.; Tang, J.; et al. 2025. Qwen2.5-vl technical report. *arXiv preprint arXiv:2502.13923*.

Chen, S.; Zhu, T.; Zhou, R.; Zhang, J.; Gao, S.; Niebles, J. C.; Geva, M.; He, J.; Wu, J.; and Li, M. 2025. Why is spatial reasoning hard for vlms? an attention mechanism perspective on focus areas. In *Proc. of ICML*.

Fu, C.; Chen, P.; Shen, Y.; Qin, Y.; Zhang, M.; Lin, X.; Yang, J.; Zheng, X.; Li, K.; Sun, X.; Wu, Y.; and Ji, R. 2024. Mme: A comprehensive evaluation benchmark for multimodal large language models. *arXiv preprint arXiv:2306.13394*.

He, J.; Zhu, K.; Guo, H.; Fang, J.; Hua, Z.; Jia, Y.; Tang, M.; Chua, T.-S.; and Wang, J. 2025. Cracking the code of hallucination in lvlms with vision-aware head divergence. In *Proc. of ACL*.

Huang, Q.; Dong, X.; Zhang, P.; Wang, B.; He, C.; Wang, J.; Lin, D.; Zhang, W.; and Yu, N. 2024. Opera: Alleviating hallucination in multi-modal large language models via over-trust penalty and retrospection-allocation. In *Proc. of CVPR*, 13418–13427.

Kang, S.; Kim, J.; Kim, J.; and Hwang, S. J. 2025. See what you are told: Visual attention sink in large multimodal models. In *Proc. of ICLR*.

Leng, S.; Zhang, H.; Chen, G.; Li, X.; Lu, S.; Miao, C.; and Bing, L. 2024. Mitigating object hallucinations in large vision-language models through visual contrastive decoding. In *Proc. of CVPR*, 13872–13882.

Li, J.; Zhang, J.; Jie, Z.; Ma, L.; and Li, G. 2025. Mitigating hallucination for large vision language model by inter-modality correlation calibration decoding. *arXiv preprint arXiv:2501.01926*.

Li, Y.; Du, Y.; Zhou, K.; Wang, J.; Zhao, W. X.; and Wen, J.-R. 2023. Evaluating object hallucination in large vision-language models. In *Proc. of EMNLP*, 292–305.

Liu, H.; Li, C.; Wu, Q.; and Lee, Y. J. 2023. Visual instruction tuning. In *Proc. of NIPS*, 34892–34916.

Liu, H.; Xue, W.; Chen, Y.; Chen, D.; Zhao, X.; Wang, K.; Hou, L.; Li, R.; and Peng, W. 2024. A survey on hallucination in large vision-language models. *arXiv preprint arXiv:2402.00253*.

Liu, S.; Zheng, K.; and Chen, W. 2024. Paying more attention to image: A training-free method for alleviating hallucination in lvlms. In *Proc. of ECCV*, 125–140.

Wang, J.; Wang, Y.; Xu, G.; Zhang, J.; Gu, Y.; Jia, H.; Wang, J.; Xu, H.; Yan, M.; Zhang, J.; et al. 2023. Amber: An llm-free multi-dimensional benchmark for mllms hallucination evaluation. *arXiv preprint arXiv:2311.07397*.

Wu, M.; Ji, J.; Huang, O.; Li, J.; Wu, Y.; Sun, X.; and Ji, R. 2024. Evaluating and analyzing relationship hallucinations in large vision-language models. In *Proc. of ICML*, 53553–53570. PMLR.

Xie, C.; Liu, T.; Jiang, L.; Zeng, Y.; Shen, Y.; Huang, W.; Li, J.; Xu, X.; et al. 2025. Tarac: Mitigating hallucination in lvlms via temporal attention real-time accumulative connection. *arXiv preprint arXiv:2504.04099*.

Yang, T.; Li, Z.; Cao, J.; and Xu, C. 2025. Understanding and mitigating hallucination in large vision-language models via modular attribution and intervention. In *Proc. of ICLR*.

Yin, H.; Si, G.; and Wang, Z. 2025a. ClearSight: visual signal enhancement for object hallucination mitigation in multimodal large language models. In *Proc. of CVPR*, 14625–14634.

Yin, H.; Si, G.; and Wang, Z. 2025b. Lifting the Veil on Visual Information Flow in MLLMs: Unlocking Pathways to Faster Inference. In *Proceedings of the Computer Vision and Pattern Recognition Conference*, 9382–9391.

Zhang, J.; Khayatkhoei, M.; Chhikara, P.; and Ilievski, F. 2025. Mllms know where to look: Training-free perception of small visual details with multimodal llms. In *Proc. of ICLR*.

Zhang, X.; Quan, Y.; Gu, C.; Shen, C.; Yuan, X.; Yan, S.; Cheng, H.; Wu, K.; and Ye, J. 2024. Seeing clearly by layer two: Enhancing attention heads to alleviate hallucination in lvlms. *arXiv preprint arXiv:2411.09968*.

Zhao, J.; Zhang, F.; Sun, X.; and Feng, C. 2025a. Aligning attention distribution to information flow for hallucination mitigation in large vision-language models.

Zhao, J.; Zhang, F.; Sun, X.; and Feng, C. 2025b. Cross-image contrastive decoding: Precise, lossless suppression of language priors in large vision-language models. *arXiv preprint arXiv:2505.10634*.

Zhu, L.; Ji, D.; Chen, T.; Xu, P.; Ye, J.; and Liu, J. 2025a. Ibd: Alleviating hallucinations in large vision-language models via image-biased decoding. In *Proc. of CVPR*, 1624–1633.

Zhu, Y.; Tao, L.; Dong, M.; and Xu, C. 2025b. Mitigating object hallucinations in large vision-language models via attention calibration. *arXiv preprint arXiv:2502.01969*.

Zou, X.; Wang, Y.; Yan, Y.; Lyu, Y.; Zheng, K.; Huang, S.; Chen, J.; Jiang, P.; Liu, J.; Tang, C.; et al. 2025. Look twice before you answer: Memory-space visual retracing for hallucination mitigation in multimodal large language models. In *Proc. of ICML*.

## A Implementation Details for Baselines

The hyperparameter settings for the baselines in our experiments are as follows:

- **VCD** (Leng et al. 2024): We add 500 steps of Gaussian noise to the original image to construct the contrastive visual input, and the hyperparameters for contrastive decoding are set to  $\alpha = 1, \beta = 0.1$ .
- **PAI** (Liu, Zheng, and Chen 2024): We activate the PAI method starting from layer 2 (counting from 0), with hyperparameters set to  $\alpha = 0.5, \gamma = 1.1$ .
- **VAR** (Kang et al. 2025): The hyperparameters in this method are set as follows:  $\tau = 20, \rho = 0.5$ , and  $p = 0.6$ .
- **AD-HH** (Yang et al. 2025): We set the hallucination threshold  $\tau$  for attention heads to 0.5. For the definition of hallucination heads, please refer to the original paper.
- **VAF** (Yin, Si, and Wang 2025a): We set  $\beta = 0.1, \alpha = 0.15$ , and activate this method from layer 9 to layer 14 (counting from 0).
- **TARAC** (Xie et al. 2025): We set  $\beta = 0.5, \alpha = 0.5$ , and activate this method from layer 9 to layer 15 (counting from 0).

**Note:** Parameters with the same name may have different meanings across methods; please refer to the original papers for their specific definitions.

## B More Experimental Results

### B.1 Results on MME

We evaluated the performance of our method on a wider range of tasks using the MME benchmark, as shown in Table 5. Our method achieves the highest overall score among all baselines, but exhibits relatively weak performance on the position perception task. We argue that the position task relies heavily on spatial information in the image, and our approach—by prolonging LVLMs’ focus on key objects—does not enhance their understanding of spatial relationships. In contrast, our method significantly improves LVLMs’ comprehension of key objects in the color, count, and OCR tasks.

### B.2 Results on POPE

The effectiveness of CLVS stems from the LVLM’s inherent attention to key objects. However, when no key objects are present in the image—such as in the negative samples of object hallucination tests—CLVS becomes ineffective. The results on POPE clearly illustrate this issue: our method significantly improves recall, *i.e.*, accuracy on positive samples, but performs poorly on negative samples, resulting in unstable improvement.

### B.3 $\gamma$ for LLaVA-Next and Qwen2.5-VL

$\gamma$  is a hyperparameter that acts as a soft window size, limiting how far the model can look back into previous layers. We search for the optimal value of  $\gamma$ , and the experimental results are shown in Figure 8. Based on the results, we set  $\gamma = 0.7$  for LLaVA-Next and Qwen2.5-VL.

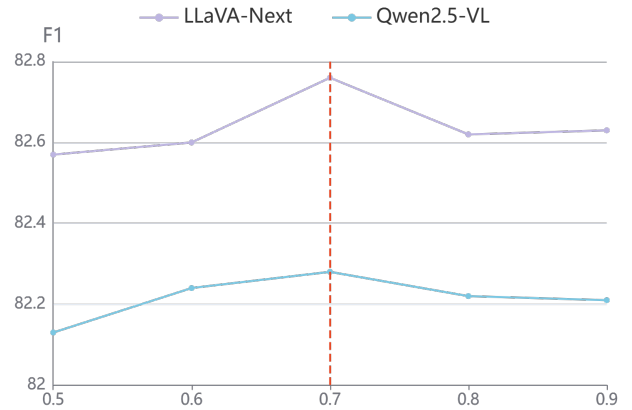


Figure 8: Effects of  $\gamma$  in LLaVA-Next and Qwen2.5-VL.

Method	Exsistence	Count	Position	Color	OCR	Total	Exsistence	Count	Position	Color	OCR	Total
	LLaVA-1.5-7B							LLaVA-1.5-13B				
Vanilla	<b>195.0</b>	158.3	123.3	155.0	125.0	756.7	<b>190.0</b>	158.3	<b>120.0</b>	160.0	132.5	760.8
VCD	185.0	158.3	123.3	146.7	122.5	735.8	<b>190.0</b>	148.3	<b>120.0</b>	155.0	140.0	753.3
PAI	185.0	151.7	<b>128.3</b>	<b>170.0</b>	132.5	767.5	<b>190.0</b>	153.3	105.0	165.0	117.5	730.8
VAR	190.0	153.3	123.3	165.0	125.0	756.7	<b>190.0</b>	153.3	<b>120.0</b>	160.0	132.5	755.8
AD-HH	<b>195.0</b>	158.3	<b>128.3</b>	165.0	125.0	771.7	<b>190.0</b>	148.3	<b>120.0</b>	160.0	132.5	750.8
VAF	190.0	151.7	128.3	155.0	<b>140.0</b>	765.0	<b>190.0</b>	163.3	<b>120.0</b>	155.0	132.5	760.8
TARAC	<b>195.0</b>	158.3	<b>128.3</b>	165.0	125.0	771.7	<b>190.0</b>	158.3	<b>120.0</b>	170.0	132.5	770.8
CLVS	<b>195.0</b>	<b>163.3</b>	123.3	<b>170.0</b>	<b>140.0</b>	<b>791.7</b>	<b>190.0</b>	<b>168.3</b>	115.0	<b>175.0</b>	<b>147.5</b>	<b>795.8</b>

Table 5: The results on MME. **Total** denotes the overall score.

Model	Method	Random			Popular			Adversarial		
		Acc.	Rec.	F1	Acc.	Rec.	F1	Acc.	Rec.	F1
LLaVA-v1.5	Vanilla	88.3	81.6	87.5	<b>85.0</b>	81.6	<b>84.5</b>	<b>81.1</b>	81.6	<b>81.2</b>
	CLVS	<b>89.0(+0.7)</b>	<b>84.5(+2.9)</b>	<b>88.5(+1.0)</b>	84.1(-1.0)	<b>84.5(+2.8)</b>	84.2(-0.3)	80.1(-1.0)	<b>84.4(+2.8)</b>	81.0(-0.2)
LLaVA-Next	Vanilla	87.4	77.1	85.9	85.5	77.1	84.2	82.3	77.1	81.4
	CLVS	<b>88.5(+1.1)</b>	<b>79.8(+2.7)</b>	<b>87.4(+1.5)</b>	<b>86.1(+0.7)</b>	<b>79.8(+2.7)</b>	<b>85.2(+1.1)</b>	<b>82.7(+0.4)</b>	<b>79.8(+2.7)</b>	<b>82.2(+0.8)</b>
Qwen2.5-VL	Vanilla	89.9	82.9	89.2	<b>87.9</b>	82.9	<b>87.3</b>	<b>84.8</b>	82.9	<b>84.5</b>
	CLVS	<b>90.2(+0.3)</b>	<b>83.1(+0.2)</b>	<b>89.4(+0.3)</b>	87.6(-0.3)	<b>83.1(+0.2)</b>	87.1(-0.2)	84.7(-0.1)	<b>83.1(+0.2)</b>	84.5(-0.1)

Table 6: The results on POPE with average scores among MSCOCO, A-OKVQA, and GQA.